Journal of the European Ceramic Society 20 (2000) 2261–2273

Bridging stresses and R-curves in ceramic/metal composites

O. Raddatz [a], G.A. Schneider [a,*], W. Mackens [b], H. Voß [b], N. Claussen [a]

[a] *Technical University Hamburg-Harburg, Advanced Ceramics Group, D-21071 Hamburg, Germany*
[b] *Technical University Hamburg-Harburg, Section of Mathematics, D-21071 Hamburg, Germany*

Received 29 September 1999; received in revised form 3 February 2000; accepted 12 February 2000

Abstract

Incorporation of metal into brittle ceramics results in an increase in fracture toughness, which can lead to an increase in strength, reliability and thermal shock resistance of the composite compared to monolithic ceramics. The basic material specific property, which controls the enhancement of the mechanical properties, is the bridging stress relation of the metal reinforcements. This relation was calculated from measured profiles of loaded cracks (COD) for fiber reinforced model composites and interpenetrating network composites in the system Al_2O_3/Al. Results are compared with directly measured bridging stress relations for the model materials. The bridging relations are further used to model the R-curve behavior of the composites which are compared with experimentally measured ones. Limitations of the applied procedure are discussed as well as the influence of specimen geometry and flaw size. © 2000 Elsevier Science Ltd. All rights reserved.

Keywords: Al_2O_3/Al; Bridging stresses; Composites; Metallic inclusions; Toughness and toughening; R-curves

Contents

* Corresponding author. Tel.: +49-40-42878-3137; fax: +49-40-42878-2647.
E-mail address: g.schneider@tu-harburg.de (G.A. Schneider).

0955-2219/00/$ - see front matter © 2000 Elsevier Science Ltd. All rights reserved.
PII: S0955-2219(00)00065-0

1. Introduction

The application of ceramic materials as structural components is often limited by their brittleness. During the last decades, different toughening mechanisms have been discovered or developed, like transformation toughening, microcracking, whisker, platelet or ceramic fiber reinforcement and the incorporation of ductile metallic phases.[1–8] As an example, experimental work on the latter case revealed clearly enhanced toughnesses of the composites compared to monolithic ceramics.[7–11] In addition, also other properties like strength, reliability and thermal shock resistance could be increased.[7,12,13]

The reason for the enhanced mechanical properties of a ceramic/metal composite is the ability of ductile metal ligaments to bridge an advancing crack in the material and to exert crack closure stresses on the crack wake.[4,11,14] The magnitude of these stresses is based upon a stress strain relation of the metal ligaments which is influenced by the properties of the reinforcing metal itself and the constraint (i.e. ligament diameter, orientation and interface properties/debonding). The shape of a crack in a component finally determines the distribution of bridging stresses along the crack faces, which in turn determines the toughness. The shape, however, is dependent on the actual crack length, the specimen and loading geometry, the bridging relation itself, and also on matrix toughness and initial flaw size. Thus, toughness is an individual property which varies from case to case. The material specific bridging relation, which is necessary to be able to predict material behavior is, however, difficult to determine experimentally or theoretically.

Much work has been done during the last decades which contributes to our current understanding of reinforcement of ceramics by ductile inclusions.[4,7,8,11,14–26] Many of these studies point out the central importance of the bridging stress relation, and efforts have been made to model or deduce this relation from direct or indirect measurements. Also its influence on toughness has been discussed and modeled. Some overview has been described elsewhere.[11]

The calculations, which will be presented in this paper, explicitly consider the interdependence of bridging stresses, crack profiles (COD) and R-curves. A method proposed by Fett will be applied, which is based on the weight function method by Bückner.[11,27,28] It is used to calculate bridging relations from COD measurements, and also to calculate R-curves from known or assumed bridging relations. Modeled results are compared with experimental results which have been obtained on Al-fiber and Al-network reinforced Al_2O_3 composites. Deviations will be discussed with respect to thermal stresses and experimental limitations. The influence of specimen geometry and initial flaw size on R-curve behavior will also be discussed.

2. Experimental

Two types of ceramic/metal composites were used for the experimental work: one being a model material with unidirectional Al-fibers of 340 and 130 μm diameter in an Al_2O_3 matrix, of which results for the 340 μm and partly for the 130 μm fibers have been presented previously,[11] and the other one being a composite with an interpenetrating network microstructure of Al and Al_2O_3 with the metal ligament diameter in the order of 1 μm. Details of the specimen preparation have been described elsewhere[7,8,11,29] and will only briefly be outlined below. Also the experimental procedures for measuring R-curves, crack opening displacements and bridging stresses can be found in more detail in Ref. 11.

2.1. Specimen preparation

In both types of composites, the porous ceramic preforms were produced from slip cast Al_2O_3 bodies. The (99.9% pure) Al reinforcements were gas pressure infiltrated at 1050 °C. The fibers in the model materials were unidirectional and equispaced with a spacing equivalent to the fiber diameter (340 and 130 μm, respectively). Two to three layers of fibers were placed on top of each other, leading to a metal volume fraction after careful grinding of approximately 13 vol%. The grain size of the Al_2O_3 matrix in these materials (Ceralox HPA 0.5) was approximately 3 μm. For the interpenetrating network microstructures, the porosity of the preforms was controlled by partial sintering, leading to a final metal volume fraction of 25 vol% after infiltration. The matrix grain size for these materials (Alcoa CT 2000 SG) as well as the metal ligament diameter was in the order of 1 μm.

2.2. R-curves

R-curves were measured using compact tension specimens. They were prepared from the composite materials by cutting and grinding. The dimensions of the specimens were chosen according to ASTM standard[30] with a specimen width, W, of 40 mm for the fiber composites and 20 mm for the network composites. The shorter width of the network materials was sufficient due to very short R-curves. The specimen thickness of all specimens was chosen between 1.8 and 3 mm, which is permitted to be much smaller than proposed in the standard because ceramics meet the requirements for plane strain conditions also for thin plates due to their very high yield stress. For the model materials the fibers were oriented perpendicular to the plane of crack extension. Precracks were grown from notches and Vickers indents into the specimens by gentle loading, and the precrack was backsawed as close as possible to the crack front in order to shorten the bridged crack

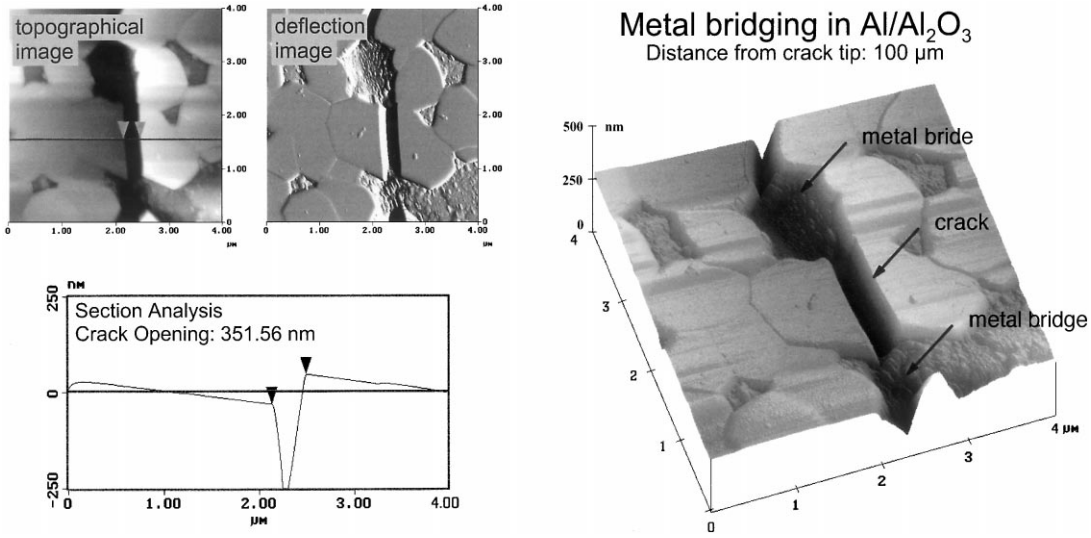

Fig. 1. AFM images of a bridged crack in an Al_2O_3/Al network composite. The section scan demonstrates the principle of COD measurement.

length before starting the experiment. For the network materials, the instability of crack growth, however, required rather long precracks of approx. 1 mm.

R-curves were measured with a stiff piezoelectric-driven double cantilever testing device (see also Ref. 11). The critical load for crack extension was recorded by an integrated load cell and the actual crack length was measured with an optical microscope. The fracture toughness was finally calculated according to Ref. 30.

2.3. Crack opening displacements

The compact tension specimens from the R-curve measurements were also used to determine the crack opening displacements (COD). The specimens were fixed at a load slightly below the critical load for crack extension (approx. 90%). The reduced load was necessary to avoid any slow crack growth during the measurement. While the fiber materials were fixed with a wedge, the network materials could be held in a miniature tensile device (Kamrath and Weiss, Germany), where also part of the crack growth was performed. To measure the COD, an atomic force microscope (dimension 3000, Digital Instruments, USA) was used, which provided an excellent resolution. Scans with a size of 1×1 up to 5×5 μm^2 were recorded at the specimen surface along the crack. The scanner was calibrated in lateral direction using a gauged 200 nm grating (Nanosensors, Dr. Olaf Walter GmbH, Germany). The crack opening between opposite located crack walls was determined from sections through topographical images of the specimen, which were placed parallel to the load line of the specimen (mode I). Fig. 1 shows an example of such a measurement in the Al_2O_3/Al network microstructure.

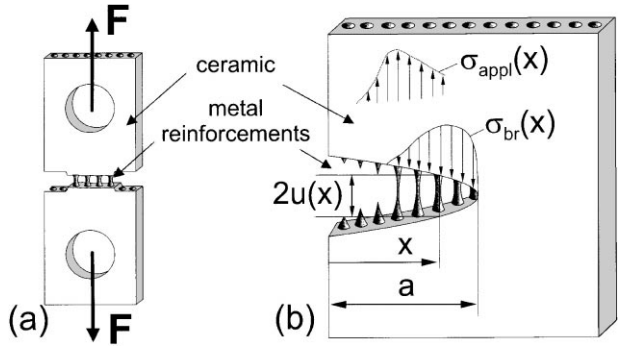

Fig. 2. Illustration of (a) specimen configuration for measuring bridging stress relations and (b) geometric relations and stresses of a cracked component.

2.4. Bridging stresses

The fiber reinforced model composite materials facilitated measurement of the bridging stress relation directly in a tensile test. Specially designed tensile bars of $24\times10\times2$ mm^3 were provided with a through the thickness matrix crack and carefully tested in tension, using the previously described R-curve device. An additional inductive displacement pick-up was mounted at the loading points above the specimen to monitor the actual crack opening. The applied force was measured by the integrated load cell. After specimen fracture, the nominal metal fraction in the cracked section was determined and the force displacement curve was recalculated and plotted as fiber bridging stress (σ_{br}) versus half crack opening (u). An illustration of the specimen geometry is given in Fig. 2(a). Measuring the bridging relation for the interpenetrating network material by the same method failed because the tiny ligaments had already failed during the precracking procedure.

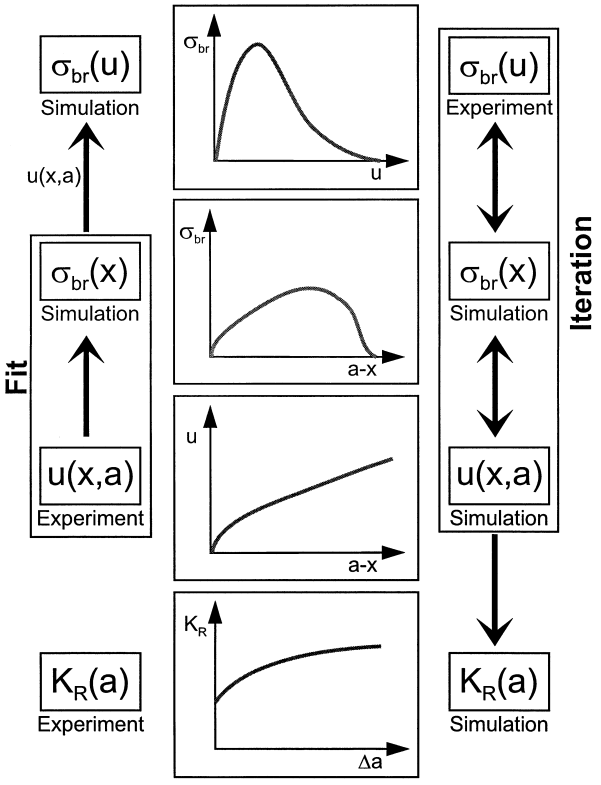

Fig. 3. Schematic of modelling principles.

3. Modeling

Modeling was performed in two main ways: (1) bridging stress relations ($\sigma_{br}(u)$) were calculated from measured crack opening displacements ($u(x,a)$), and (2) crack opening displacements ($u(x,a)$) and R-curves ($K_R(a)$) were calculated from bridging stress relations ($\sigma_{br}(u)$). This is schematically illustrated in Fig. 3, while Fig. 2(b) shows the basic geometry and stresses in a cracked specimen. The calculations are based on a theoretical approach by Fett[27] who uses the weight function method by Bückner[28] to correlate bridging stresses, crack opening displacements and R-curves in ceramics. The theoretical background has been extensively described in Refs. 11 and 31, so that only the basic relations will be outlined below.

3.1. Determination of bridging stresses

Based on a relation by Rice,[32] the crack opening displacement can be related to the stresses along the crack by the following equation:[11,27]

$$u(x,a) = \frac{1}{E'} \cdot \int_x^a g(x,a') \cdot \int_0^{a'} g(x',a') \cdot \left[\sigma_{appl}(x') + \sigma_{br}(x')\right] dx' da' \quad (1)$$

with $E' = E$ for plane stress and $E' = E/(1\text{-}\nu^2)$ for plane strain (E is Young's modulus, ν is Poisson's ratio), u, x and a as illustrated in Fig. 2(b) and σ_{appl} being the externally applied stress and σ_{br} being the bridging stress distribution. The function $g(x,a)$ is a geometry dependent weight function, which is known and reported for many geometries.[33,34] Since the bridging stresses generally act in the opposite direction to the applied stresses, they tend to reduce the crack opening $u(x,a)$ compared to a material without bridging stresses. The inner integral over the applied stresses in Eq. (1) can be replaced by a function of the applied stress intensity at the given crack length a, $K_{appl}(a)$, which can easily be determined from the applied load during the measurement.[11] So knowing $K_{appl}(a)$ and measuring the crack opening displacement $u(x,a)$, Eq. (1) can be used to calculate the corresponding distribution of bridging stresses. Combining $\sigma_{br}(x)$ and the measured crack profile $u(x,a)$, the general bridging stress vs crack opening relation, $\sigma_{br}(u)$, can be determined.

Solving Eq. (1) for the unknown bridging stresses, however, causes severe mathematical difficulties, because it formally requires a differentiation of the measured crack profile. Since $u(x,a)$ is always subjected to measuring errors, these errors will be enhanced and, in the worst case, lead to a highly oscillating and non-physical bridging stress distribution. Another problem is the fact that the crack profile in general is not particularly sensitive to local variations in bridging stresses. Smoothing the profile before starting the calculation is difficult, because the type of smoothing can significantly alter the resulting bridging stresses. Also smoothing of the calculated bridging stress distribution by a regularization method[11,22] did not work in all cases. To the experience of the authors, the most reliable method is to limit the shape and the degree of freedom of the expected bridging stress distribution to a minimum and to optimize its parameters according to the measured crack profile. This method, of course, requires a physical or engineering idea of how the bridging relation will look like in principal. In our case, a linear increase of the bridging stress with crack opening up to a maximum stress, followed by a linear decrease until ligament fracture, was chosen. This was done on the basis of experimental results, which have previously been published on the 340 and 130 μm Al-fiber model materials.[11] The complete bridging relations, measured from the initial opening of the crack up to the final ligament failure clearly revealed this general shape of the bridging relation. So Eq. (1) was solved from right to left, and the error compared to the measured crack profile was minimized by optimizing the position and magnitude of the maximum bridging stress and the crack opening at fiber fracture.

For all calculations, the weight function $g(x,a)$ for the CT-specimen was calculated in accordance with

Fett.[34,11] The measured Young's moduli were 396 and 263 GPa for the monolithic Al_2O_3 and the network composite, respectively. For the model composites, Young's modulus was estimated by the rule of mixture, $E=(1\text{-}f_{met})\cdot E_{Al_2O_3}+f_{met}\cdot E_{Al}$, with $E_{Al}=72$ GPa and a metal fiber fraction of $f_{met}=0.13$. Poisson's ratio was taken as $\nu=0.25$ to correct Young's modulus for plane strain according to $E'=E/(1\text{-}\nu^2)$.

3.2. Determination of R-curves

By applying the weight function method, one can calculate the increase in fracture toughness for a given crack length, a, when the distribution of bridging stresses along the crack, $\sigma_{br}(x)$, is known. Then, the toughness or R-curve can be calculated according to Eq. (2), where the crack tip toughness is set equal to the intrinsic toughness, K_{I0}, of the composite.[11]

$$K_R(a) = K_{I0} - \int_0^a g(x,a)\cdot\sigma_{br}(x)\mathrm{d}x \quad (2)$$

Starting with a physically plausible (or measured) bridging stress relation, $\sigma_{br}(u)$, the stress distribution along the crack, $\sigma_{br}(x)$, must first be determined for each individual crack length, geometry and K_{I0}. Therefore, a self consistent crack profile, $u(x,a)$, has to be determined from Eq. (1). In that case, $\sigma_{br}(x')$ is written as $\sigma_{br}(u(x',a))$ and σ_{appl}, as before, is replaced by a function of $K_{appl}(a)$. In that case the latter is equal to $K_R(a)$ as defined by Eq. (2) (for details see Ref. 11). The resulting equation can be solved iteratively, starting from a square root shaped COD without bridging stresses, which finally converges towards the equilibrium COD, $u(x,a)$, and bridging stress distribution, $\sigma_{br}(x)$. K_R is then calculated point by point, using different crack length a.

4. Results

4.1. Crack path

Fig. 1 shows an AFM image of the surface of an Al_2O_3/Al composite with an interpenetrating network microstructure. While the flat and faceted shaped Al_2O_3 grains are clearly visible, the Al phase appears more rough and somewhat deeper due to polishing. The image clearly shows the presence of metal ligaments, bridging the crack in the material. Those ligaments are deeper compared to the surrounding, unaffected metal pockets because they plastically deform and neck in order to bridge the gap between opposing crack walls. For the fiber reinforced model materials, the bridging ligaments were not visible in the AFM images, because they are surrounded with Al_2O_3 matrix and are located below the surface. The crack path which was followed and measured on the Al_2O_3 surface meandered mainly along the grain boundaries in Al_2O_3.

Even though the bridging sites are at discrete locations along the crack faces, because of the considerable thickness of the specimens, the close spacing of bridging sites and the high stiffness of the ceramic matrix we regarded the bridging stresses as if they were continuously distributed. Because of the high matrix stiffness, we also neglected possible surface effects, which, from an unpublished work by Göken et al. on materials with comparable dimensions and elastic properties, showed to be at least an order of magnitude smaller than the resolution in crack opening achieved with the AFM. This resolution, however, is difficult to quantify. While the nominal resolution of the AFM for the evaluation of topographical sections is as small as 2 nm for 1×1 μm^2 scans, defining the edges of a crack is sometimes difficult due to rough surfaces or damaged edges and the limited curvature of the needle tip (about 10 nm radius). From our experience, we estimate that the resolution which can be achieved is in the order of 20 nm for half crack opening displacements below 100 nm and may be up to 50 nm for large COD's of >1 μm.

4.2. Correlation of COD, bridging stresses and R-curves

Using the techniques described in the previous sections, CODs were measured for the fiber and for the network composites. Fig. 4 shows such a measurement for the Al_2O_3/Al composite with the interpenetrating network microstructure. Also shown in this figure is the theoretical crack profile after Eq. (1) for the applied stress intensity of 4.2 MPa$\sqrt{}$m (upper solid line, no bridging stresses) and the near tip square root shaped profile for an intrinsic toughness of $K_{I0}=2.4$ MPa$\sqrt{}$m (lower solid line). As can be seen in Fig. 4, the measured COD remains well below the K_{appl} displacements due to the presence of bridging stresses. Also shown in this figure are fitted profiles (labeled ①–③) to the measured COD, which were determined using different boundary conditions for the bridging stress relation. They will be explained in the discussion. An example for a COD measurement in the 340 μm Al-fiber material is given elsewhere.[11]

From all COD measurements on the different materials, the bridging stress distributions were calculated and, respecting the metal volume fractions, transformed into material specific bridging relations, $\sigma_{br}(u)$, of the metal ligaments. A bridging relation for interlocking matrix grains could also be calculated for a monolithic alumina. The calculated results are plotted in Fig 5 together with experimental bridging relations obtained for the model materials. The experimental curves show initially a fairly linear rising part up to a maximum stress of around 90 MPa, before they decrease to zero

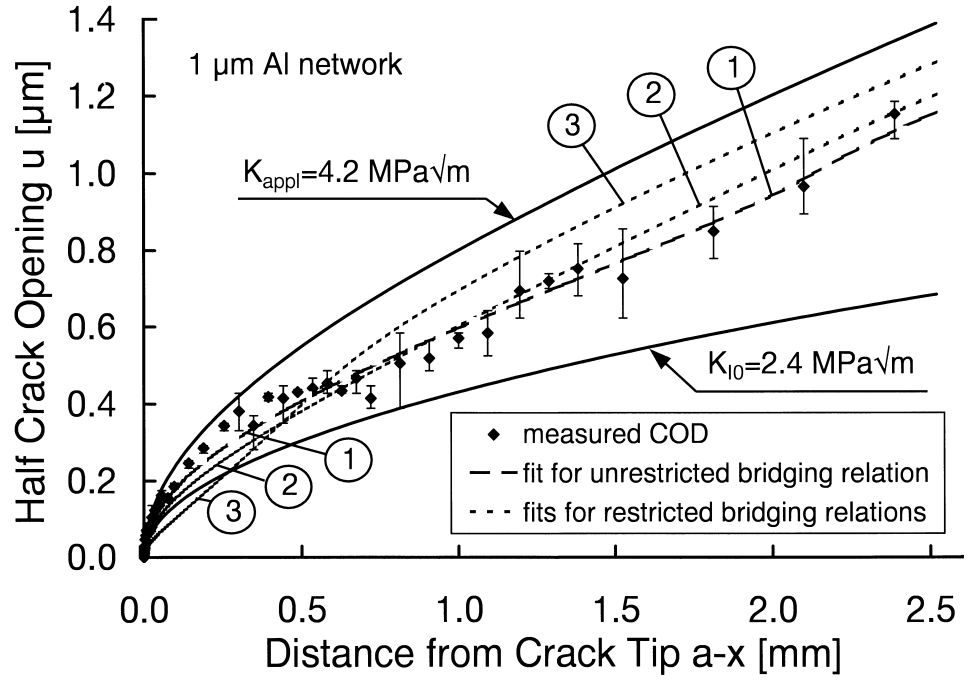

Fig. 4. Example of measured crack opening as a function of distance from the crack tip for the Al_2O_3/Al network composite.

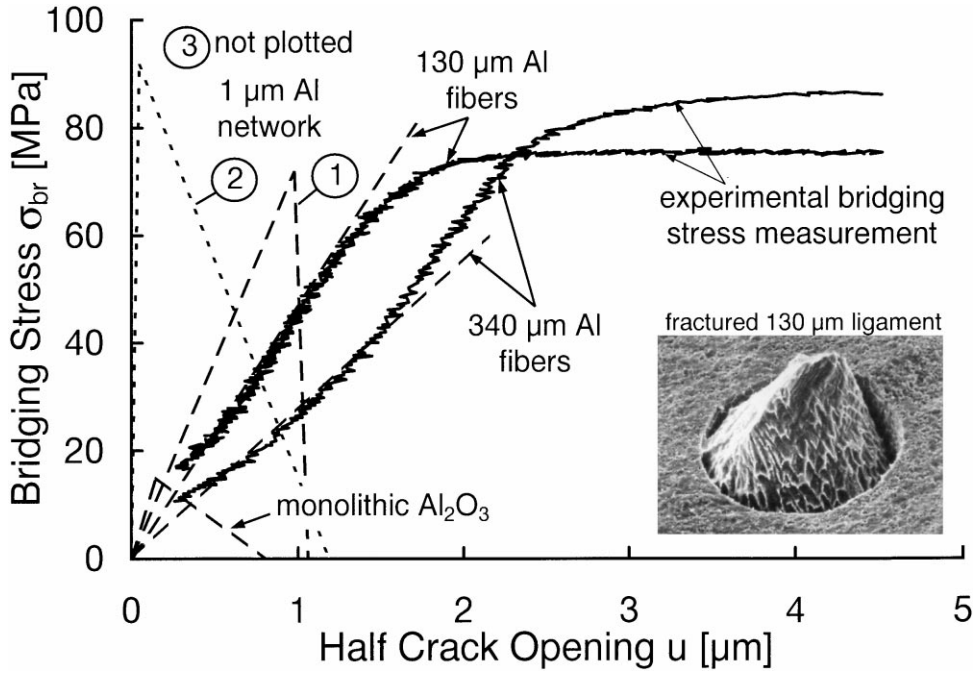

Fig. 5. Measured and calculated bridging stress relations of metal ligaments and ceramic grains (dashed lines: calculated from COD).

stress at fiber fracture (outside the plot of Fig. 5) at a crack opening roughly in the order of the fiber diameter itself. This was already determined in Ref. 11. Also visible is the fact that the bridging relation is shifted to smaller displacements for the smaller fiber diameters. The general shape of the bridging relation as experimentally obtained was also used for calculating the bridging stresses from COD measurements, as mentioned in Section 3.1. All relevant results of the experimental measurements and the modeling are summarized in Table 1.

The limit up to which the bridging stress relation can be calculated is given by the largest crack opening achieved during the COD measurement. In ceramics and ceramic composites, even for long crack lengths, this hardly exceeds a few micron. For the model materials, the maximum half crack openings were 2.2 and 1.7 µm

for the 340 and 130 μm fiber materials, respectively, and the calculated bridging stresses resulted to be completely within the linear region of the bridging stress relation. For the network material, the complete bridging relation, including the decreasing part of the curve, could be calculated (① in Fig. 5). Additional boundary conditions were introduced to calculate the bridging relations labeled ② and ③. This will be discussed in Section 5.

Using the averaged experimentally determined bridging relations of the model materials and the calculated one for the network material, R-curves were generated for these materials. They are plotted in comparison to experimental R-curves in Fig. 6. It turned out that for the model materials, grain bridging of the ceramic matrix had to be included into the bridging relation in order to account for the toughness increase at short crack length. The presence of such bridges is a well known phenomenon[35,36] and was also obvious from a measured R-curve in a monolithic alumina of the same type, which clearly showed an R-curve behavior (see Fig. 6). While the R-curves of the model materials are continuously rising, still being far away from their plateau values, the rising part of the R-curve in the network material was not resolved, because the required starting crack length was too long. Only the plateau toughness could be measured in that case. This is not specific to the used CT-specimen configuration, but is a common and general problem also with other specimen configurations or testing methods.

This also leads to the problem that the starting value of the R-curves (K_{I0}) can not be determined from the R-curve measurements because of the finite starting crack length. Instead, K_{I0} was estimated from the near tip profiles of the COD measurements. For the model materials, this toughness was determined to be approximately 2.4 MPa$\sqrt{m}$, while for the network material it turned out to be in the order of 3.2 MPa$\sqrt{m}$.

The algorithm for calculating R-curves from bridging stress relations was further used to demonstrate the influence of specimen geometry and initial crack length

Table 1
Comparison of measured and calculated bridging stress relations in Al_2O_3/Al

Material	Method	Initial slope (MPa/μm)	Max. stress (MPa)	Crack opening ($2u$) at max. stress (μm)	Crack opening ($2u$) at lig. failure (μm)
340 μm Al fiber	Experiment	32.1±5.7	90±8	11.7±3.1	202±46
	calculated from COD	27.9	(60)		
130 μm Al fiber	Experiment	53.5±16.0	92±14	5.2±1.2	95±14
	calculated from COD	47.0	(81)	–	–
1 μm Al network	Calculated from COD	73.4	72	1.9	2.1

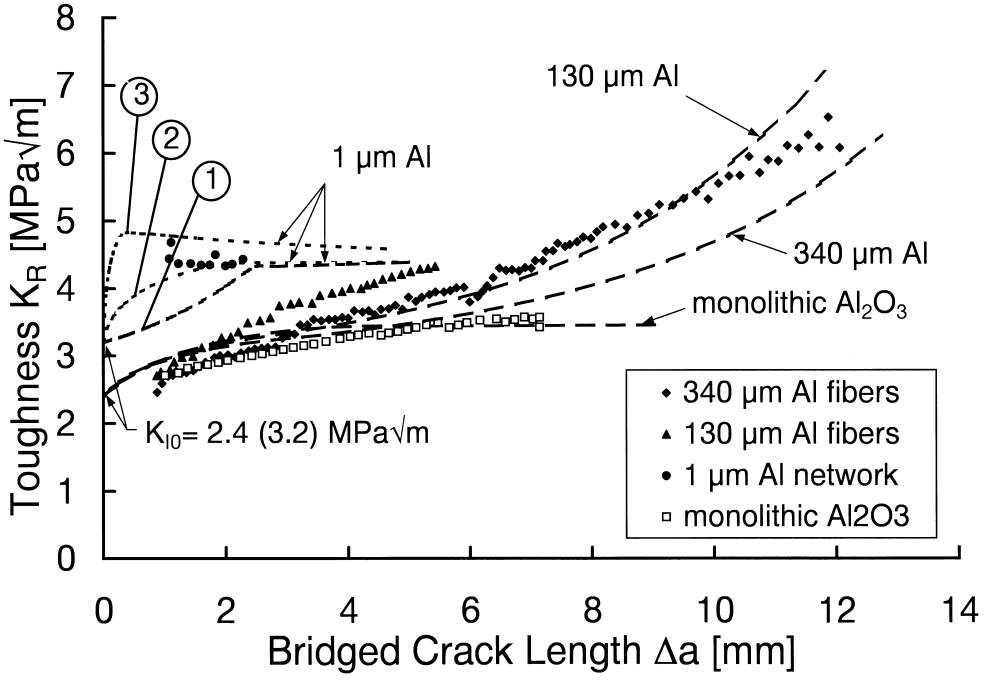

Fig. 6. Measured R-curves (symbols) and calculated R-curves (lines) for Al_2O_3/Al composites and monolithic Al_2O_3.

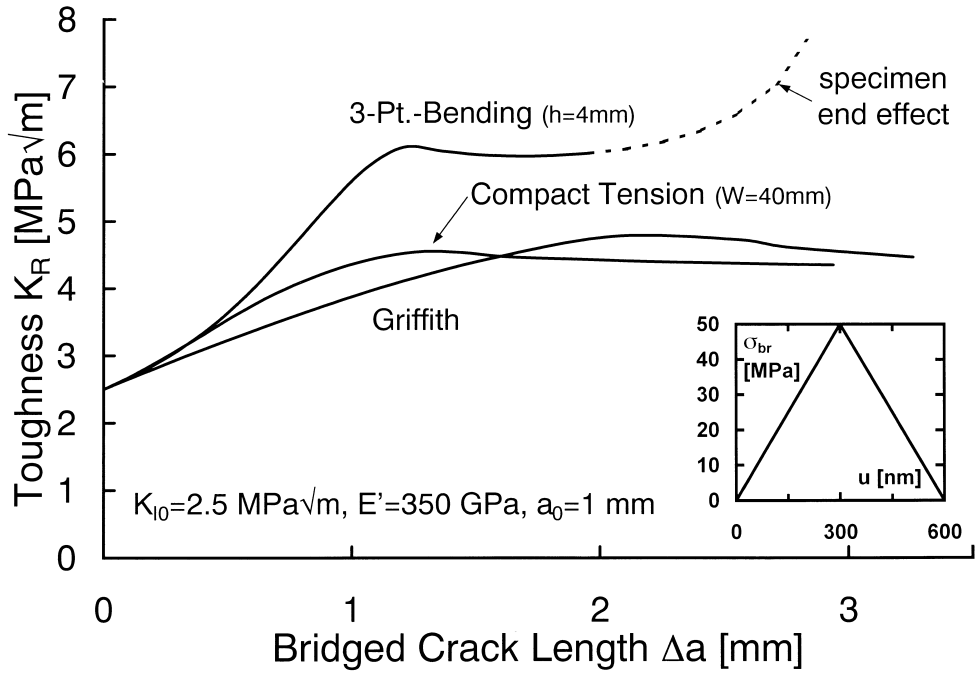

Fig. 7. Calculated R-curves demonstrating the influence of specimen geometry.

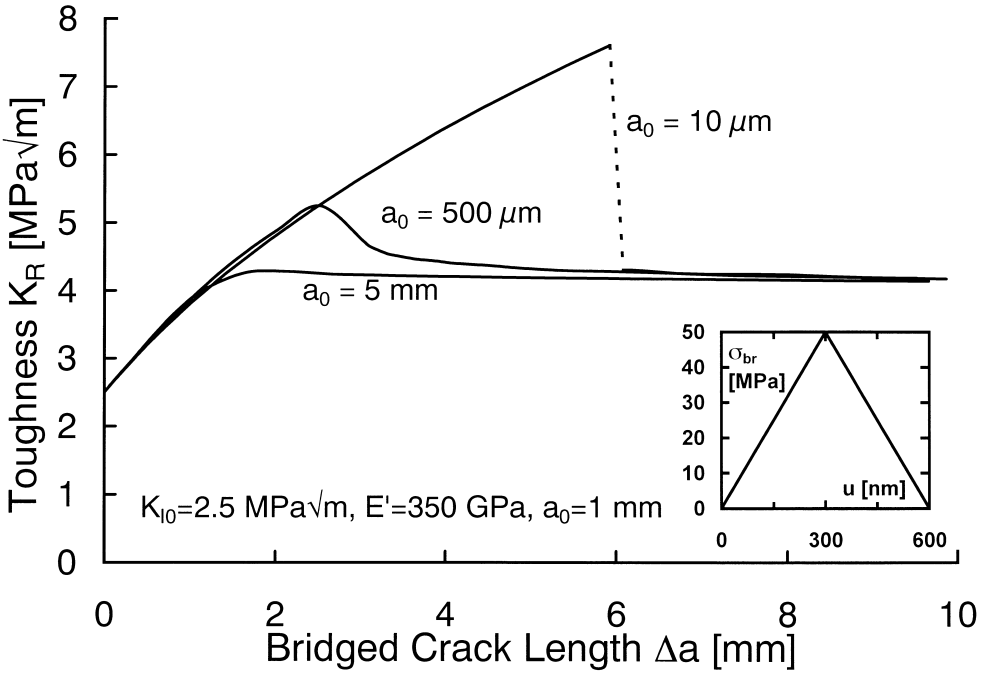

Fig. 8. Calculated R-curves demonstrating the influence of initial flaw size and the presence of unstable R-curves for small flaw sizes.

on R-curve behavior. For this purpose, a simple bridging relation, increasing linearly from zero to a maximum average stress of 50 MPa at a half crack opening of 300 nm, followed by a linear decrease to zero stress at a half crack opening of 600 nm, was assumed. The resulting R-curves for a bending, compact tension and infinite specimen under uniform tension (Griffith geometry) are plotted in Fig 7. The corresponding weight functions are reported in Ref. 34. The influence of initial crack length or flaw size is demonstrated for the Griffith geometry in Fig 8. The R-curves show a pronounced maximum and instability for small flaw sizes. Details on those results will be explained and commented on in the discussion.

5. Discussion

The results demonstrate that CODs, R-curves and bridging stresses can be correlated with the applied algorithms. Bridging relations were calculated from COD measurements, and R-curves were calculated from bridging relations. Regarding the calculated bridging stress relations, the results are in very good agreement with experimentally measured bridging relations for the model materials. This also confirms the result which was previously given for the 340 μm model material in Ref. 11, where the bridging relation was determined using a more general approach for the shape of the bridging relation and applying a regularization method. The observed linearity for the initial part of the curves was also reported in earlier works[8,14,29] and the maximum fiber stress lies well above the bulk strength of pure aluminum due to the constraint. Due to some debonding during the fracture process (see e.g. fracture image in Fig. 5), the stress increase was not as high as reported e.g. in Refs. 8 and 14. As already proposed by Ashby et al.,[14] the bridging stress relation is shifted to lower values of displacements for smaller ligament diameters. This might be explained by a higher constraint and a smaller metal volume which can plastically deform and bridge the crack. While the crack opening at fiber fracture seems to scale directly with fiber diameter (d), the linear rising slope of the measured bridging relations seems to scale more with a factor of $1\sqrt{d}$. The mechanism which controls the initial part of the bridging stress relation is not yet understood, and no theoretical model can be offered at this point neither for the initial linear part of the curve nor for the linear decreasing part. It is also unclear if plastic deformation is already involved in the initial part of the curves, or if the behavior is fully elastic. Pure elasticity would require unexpected long debond lengths of many times the fiber diameter in order to explain the measured slopes. An approach, how such long debond length might develop under the given constraint due to thermal mismatch stresses is given elsewhere.[37] The decreasing part of the curves is, however, expected to occur due to a severe necking of the ligaments down to fracture.

The calculated bridging relation for the network material, however, is unexpected. Since the ligament diameter is in the order of only 1 μm, it is not probable that the reinforcements exhibit their maximum stress at a half crack opening of roughly 1 μm and then drastically drop their stress to zero (dashed line in Fig. 5 labeled ①). From the experimental results on the fiber materials and observations of fracture surfaces it seems as if (for the limited debonding observed in Al_2O_3/Al composites) fibers can be expected to bridge a crack up to crack openings which are in the order of the size of the ligament diameter. Considering that some ligaments of the network might easily have diameters up to 2 μm, it can be reasonable to have bridging stresses up to a half crack opening of 1 μm, as calculated. The maximum stress, however, is expected at an elongation of only some percent of the (average) ligament diameter (roughly 5% from the fiber experiments). To check the influence of other, more probable bridging relations on the fitting procedure of the COD, we forced the program to (1) locate the maximum bridging stress at $u = 0.05$ μm and (2) locate the maximum bridging stress at u = 0.05 μm *and* limit the presence of bridging stresses up to 2 $u = 1.0$ μm. The resulting bridging relations and fits for the COD are plotted as dotted lines in Figs. 4 and 5 and are labeled ② and ③, respectively. The result for the original, unrestricted fit, is given as the dashed line ①. The bridging relations, representing the best possible fits on the measured COD under the given boundary conditions, are quite different. While fixing the position of the stress maximum to $u = 0.05$ μm slightly rises the stress magnitude to around 90 MPa but keeps the crack opening at ligament failure almost unchanged ($u = 1.2$ μm), limiting also the position of ligament failure increases the stress magnitude to a maximum of 360 MPa (outside the range of Fig. 5, not plotted). The corresponding fit of the COD naturally becomes worse, from a very good fit for the unrestricted solution to an obvious discrepancy for the most limited solution. The average deviation $<\Delta u>$ of the calculated half crack opening displacement $u(x_i)_{\text{fit}}$ at the positions x_i to the measured N data points $u(x_i)_{\text{measured}}$

$$<\Delta u> \equiv \sqrt{\frac{\sum_{i=1}^{N}[u(x_i)_{\text{measured}} - u(x_i)_{\text{fit}}]^2}{N}} \tag{3}$$

increases at the same time from 28 to 90 nm. The deviation becomes even more pronounced when only the bridging part, $u_{\text{br}}(x)$, of the COD is plotted (Fig. 9). So the "restricted" solutions (② and ③) are certainly beyond possible measuring errors of the COD, and the original bridging stress relation (①) really seems to be more or less the best result to be obtained. Now what can then be a reason for the unexpected result? There is still one uncertainty in the measurement which can not be avoided: the influence of decreasing the applied load in order to obtain a stable crack configuration for the measurement. It is unknown how the bridging stresses react, and if their distribution might be significantly altered. The surprisingly low deviation of the COD from the applied COD close to the crack tip might for example be due to disproportionate relaxation of bridging stresses in that region or even crack opening stresses due to loosen matrix grains which felt into the crack. Finally one has to consider, that the network represents a variety of ligament diameters and orientations along the crack, resulting in individual bridging relations along

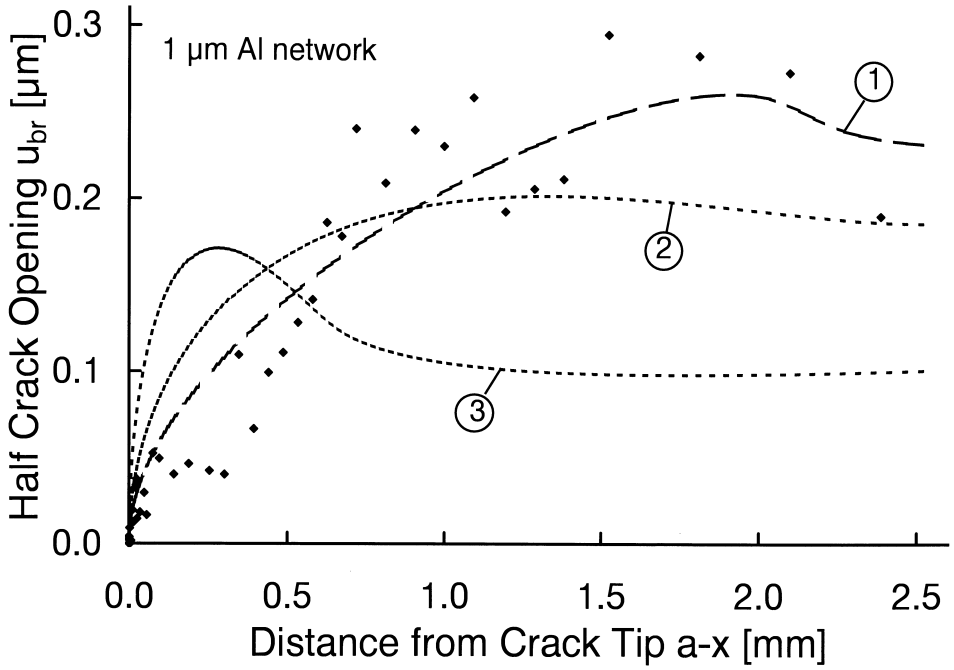

Fig. 9. Contribution to the crack opening displacement of the Al_2O_3/Al network composite caused by bridging stresses and corresponding modelled displacements for different bridging relations (symbols: measured from COD).

the crack, which might not be summarized and averaged in the same way as for the uniform model materials.

Another point, which has not been taken into account, is the influence of thermal mismatch stresses. They result from a thermal expansion mismatch between the matrix and the ligaments during processing. Because of the strong interfacial bonding in the system Al_2O_3/Al and the resulting constraint, such stresses can be significant (up to several hundred MPa) as has been reported for the network materials.[38] Anyway, such stresses were neglected in the present study for the calculation of bridging stress, assuming zero bridging stress at zero crack opening, although some earlier theoretical studies suggested that they have to be added on top of the bridging relation.[39] Instead the authors believe, that such stresses will not influence the bridging stresses in the crack wake, because the intersection of the ligaments with the crack will release the constraint and lead to a relaxation of the mismatch stresses (inducing some yielding in the ligaments). The experimental bridging stress measurements also support this view, because low stresses were required for the onset of crack opening. Evaluation of the experiments for stresses below 20 MPa is, however, difficult due to overlapping settlement of the device.

Regarding the R-curves for the three discussed bridging relations of the network material, the originally obtained bridging relation again gives a rather unlikely result (dashed line, ①). While the plateau value of the R-curve is rather well predicted, the increase of the R-curve over a distance of more than 2 mm was not found experimentally. Although the rising part of the R-curve could not be measured experimentally, the plateau toughness was already reached after less than 1 mm of crack growth. Other investigations on comparable materials using shorter initial crack length reveal a length of the R-curve of only 300 µm.[40,41] So the other bridging relations, which are thought to be more realistic, also seem to give a much better estimation of the R-curve (dotted lines, ② and ③), although a direct comparison for the first mm of crack growth is not possible. The R-curves for the model materials on the other hand are reasonably well predicted but somewhat underestimated by the calculation from the measured bridging relation. They clearly reveal that the large size of the metal ligaments significantly influences the toughness only for long crack length and large crack openings, respectively.

The fact that the initial toughness in the network material was found to be higher than that in the model materials might be explained by the higher metal volume fraction (25 compared to 13 vol%) and the interconnected microstructure of the metal. Although the influence of a second phase on K_{I0} is not yet understood, micrographs revealed that the crack tip in the network materials was always located in the metal phase, which can be thought to increase K_{I0}. The presence of significant thermal mismatch stresses ahead of the crack tip (compressive in the matrix) might also have an effect.

The influence of specimen geometry on the R-curves, as demonstrated in Fig. 7, can be quite dominant, although the bridging relations are identical. This was also reported by other authors.[25,42–44] The reason is due to the increasing rotational part on the loading of the

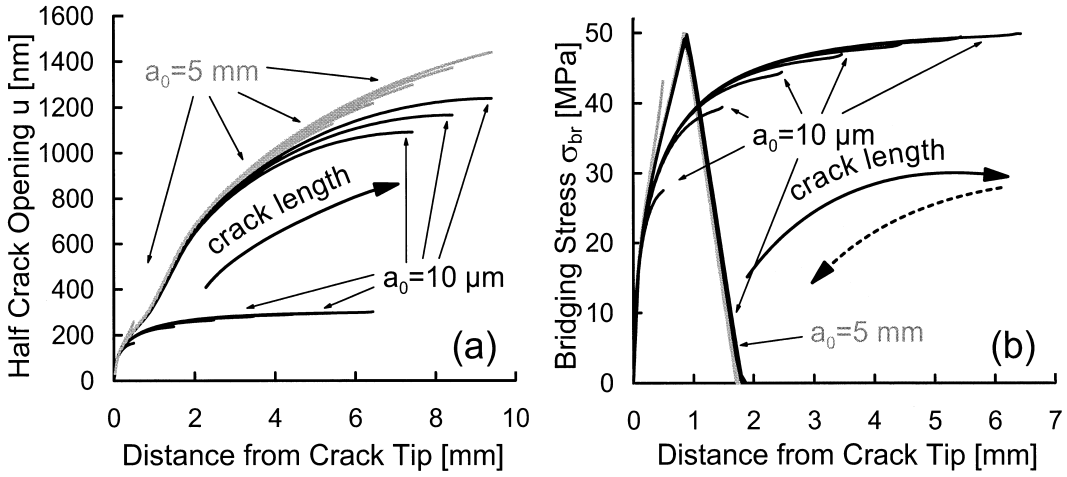

Fig. 10. Development of crack opening displacement and bridging stress distribution for flaw sizes of 10 μm and 5 μm in Griffith geometry.

crack compared to pure tension when moving from a Griffith geometry to a bending bar. Thus the crack shape is different, being further opened with increasing rotation and leading to higher bridging stresses for the given case. So the toughness can be significantly overestimated with a laboratory testing method compared to its appearance in reality.

The influence of initial crack size a_0, corresponding to the flaw size in a real component, becomes particularly interesting (Fig. 8). As could be demonstrated, the R-curve can significantly rise above the plateau level for short initial crack length, and develop a point of instability in crack shape and toughness. This behavior has also been reported and referred to as "snap-back softening" in the context of concretes[45–47] and was also reported by Erdogan and Joseph[48] and by Cox and Marshall on considering strength and fatigue.[49–51] The reason for the different behavior compared to a configuration with a large a_0 is again the difference in crack shape and corresponding bridging stress distribution (Fig. 10). For short a_0, the crack becomes fully bridged, with high bridging stresses acting over a long distance along the crack. Only when the first fiber exceeds its maximum stress (i.e. the half crack opening exceeds 300 nm), the crack is not supported with a continuously increasing bridging stress any more. The crack profile then changes significantly and a kind of chain reaction starts, leading to the failure of a large number of ligaments. For example, in Fig. 10a it can be seen that, for the case of $a_0 = 10$ μm, the crack opens only slightly ($u < 300$ μm) to a crack elongation of up to~6.5 mm. The corresponding distribution of bridging stresses is plotted in Fig. 10b, showing high bridging stresses acting along the whole crack length. Increasing the crack length by only a small increment Δa, the crack changes its shape completely. The crack opens much wider, and all ligaments where the opening exceeds $u = 600$ nm break. So the bridged crack length shortens from previously ~6.5 to~2 mm (Fig. 10b). As a consequence, the resulting fracture toughness drops significantly. With further increasing crack length, the crack profile and bridging stress distribution and the toughness remain almost constant. For long initial crack length, the crack can not develop this kind of fully bridged configuration in the beginning. The crack is far opened from the beginning, leading to an early failure of ligaments and a monotonous and stable development of a steady crack shape, bridging stress distribution and fracture toughness. The location, magnitude and appearance of the instability is certainly dependent on the bridging relation. It will be less pronounced for a smoother transition from increasing stress to decreasing stress.[48] It has to be mentioned that for the selected case (Griffith geometry, $a_0 = 10$ μm), the instability in toughness can not be reached by stable crack growth, so it will have no influence on the final performance of a component. The specimen will fail catastrophically before the high toughness is reached. However, other specimen and loading configurations might apply, where such an instability can be relevant.

6. Conclusions

R-curves, crack opening displacements and bridging stresses were measured for Al_2O_3/Al composites with different microstructures. They were correlated by applying the weight function method. Calculating bridging stresses from COD measurements led to very good results for the fiber reinforced model microstructures. For network microstructures, however, the result was rather unlikely. So difficulties in applying this method can be summarized as follows: (1) the COD is in general not particularly sensitive to small differences in bridging stress distributions. That means that a rather good knowledge of the principal type of bridging relation is required in order to obtain a

reasonable result, and (2) measuring the COD with high precision can not account for uncertainties in stress configuration and relaxation phenomena.

It was further demonstrated how R-curves can be generated with the knowledge of the material specific bridging stress relation. Using appropriate bridging relations, measured and approximated R-curves for the different Al_2O_3/Al microstructures could be simulated. Large variations in R-curve behavior for different specimen geometries and flaw sizes were demonstrated for a selected bridging relation. It emphasizes that the bridging relation of the reinforcing ligaments is the basic material property and that individual boundary conditions determine the resulting crack shape, bridging stress distribution and fracture resistance for a component. The discussed algorithm provides a method to individually account for all these parameters.

Acknowledgements

The authors gratefully acknowledge financial support of this project by the German Foundation of Research (DFG) within the "SFB 371: Micromechanics of Multiphase Materials (B5)" and contributions to the AFM work by U. Köpke.

References

1. Evans, A. G. and Heuer, A. H., Review-transformation toughening in ceramics: martensitic transformations in crack-tip stress fields. *J. Am. Ceram. Soc.*, 1980, **63**(5-6), 241–248.
2. Rühle, M., Claussen, N. and Heuer, A. H., Transformation and microcrack toughening as complementary processes in ZrO_2-toughened Al_2O_3. *J. Am. Ceram. Soc.*, 1986, **69**(3), 208–212.
3. Claussen, N., Microstructural Design of Zirconia-Toughened Ceramics (ZTC). In *Advances in Ceramics 12 (Science and Technology of Zirconia II)*, ed. N. Claussen, M. Rühle and A. H. Heuer. The American Ceramic Society, Columbus, Ohio, 1983, pp. 325–351.
4. Sigl, L. S., Mataga, P. A., Dalgleish, B. J., McMeeking, R. M. and Evans, A. G., On the toughness of brittle materials reinforced with a ductile phase. *Acta Metall.*, 1988, **36**(4), 945–953.
5. Flinn, B. D., Rühle, M. and Evans, A. G., Toughening in Composites of Al_2O_3 reinforced with Al. *Acta Metal.*, 1989, **37**(11), 3001–3006.
6. Bannister, M., Shercliff, H., Bao, G., Zok, F. and Ashby, M. F., Toughening in brittle systems by ductile bridging ligaments. *Acta Metall. Mater.*, 1992, **40**(7), 1531–1537.
7. Prielipp, H., Knechtel, M., Claussen, N., Streiffer, S. K., Müllejans, H., Rühle, M. and Rödel, J., Strength and fracture toughness of aluminum/alumina composites with interpenetrating networks. *Materials Science and Engineering*, 1995, **A197**, 19–30.
8. Hoffman, M., Fiedler, B., Emmel, T., Prielipp, H., Claussen, N. and Rödel, J., Fracture behavior in metal fibre reinforced ceramics. *Acta Mater*, 1997, **45**(9), 3609–3623.
9. Rödel, J., Prielipp, H., Claussen, N., Sternitzke, M., Alexander, K. B., Becher, P. F. and Schneibel, J. H., Ni_3Al/Al_2O_3 Composites with Interpenetrating Networks. *Scripta Metallurgica et Materialia*, 1995, **33**(5), 843–848.
10. Garcia, D. E., Schicker, S., Bruhn, J., Janssen, R. and Claussen, N., Processing and mechanical properties of presureless-sintered Nb–Al_2O_3-matrix composites. *J. Am. Ceram. Soc.*, 1998, **81**(2), 429–433.
11. Raddatz, O., Schneider, G. A. and Claussen, N., Modelling of R-curve behaviour in ceramic/metal composites. *Acta Mater*, 1998, **46**(18), 6381–6395.
12. Knechtel, M., Claussen, N. and Rödel, J., Reliability of structural ceramics. *Phil. Trans. R. Soc. Lond., A*, 1995, **351**, 469–483.
13. Schön, S., Prielipp, H., Janssen, R., Rödel, J. and Claussen, N., Effect of microstructural scale on thermal shock resistance of aluminium-reinforced alumina. *J. Am. Ceram. Soc.*, 1994, **77**(3), 701–704.
14. Ashby, M. F., Blunt, F. J. and Bannister, M., Flow characteristics of highly constrained metal wires. *Acta Metal.*, 1989, **37**(7), 1847–1857.
15. Evans, A. G., Perspective on the development of high-toughness ceramics. *J. Am. Ceram. Soc.*, 1990, **73**(2), 187–206.
16. Bao, G. and Suo, Z., Remarks on crack-bridging concepts. *Appl. Mech. Rev.*, 1992, **45**(8), 355–366.
17. Mataga, P. A., Deformation of crack-bridging ductile reinforcements in toughened brittle materials. *Acta Metall.*, 1989, **37**(12), 3349–3359.
18. Evans, A. G. and McMeeking, R. M., On the toughening of ceramics by strong reinforcements. *Acta Metall.*, 1986, **34**(12), 2435–2441.
19. Hsueh, C.-H. and Becher, P. F., Some considerations of bridging stresses for fiber-reinforced ceramics. *Composites Engineering*, 1991, **1**(3), 129–143.
20. Hay, J. C. and White, K. W., Grain boundary phases and wake zone characterization in monolithic alumina. *J. Am. Ceram. Soc.*, 1995, **78**(4), 1205–1232.
21. Kagawa, Y. and Sekine, K., Toughening by continuous single fiber bridging in ceramic matrix composite. *Materials Science and Engineering*, 1996, **A221**, 163–172.
22. Cox, B. N. and Marshall, D. B., The determination of crack bridging forces. *International Journal of Fracture*, 1991, **49**, 159–176.
23. Fett, T., Munz, D., Yu, C.-T. and Kobayashi, A. S., Determination of bridging stresses in reinforced Al_2O_3. *J. Am. Ceram. Soc.*, 1994, **77**(12), 3267–3269.
24. Fett, T., Munz, D., Thun, G. and Bahr, H. A., Evaluation of bridging parameters in aluminas from R-curves by use of the fracture mechanical weight function. *J. Am. Ceram. Soc.*, 1995, **78**(4), 949–951.
25. Fett, T., Munz, D., Seidel, J., Stech, M. and Rödel, J., Correlation between long and short crack R-curves in alumina using the crack opening displacement and fracture mechanical weight function approach. *J. Am. Ceram. Soc.*, 1996, **79**(5), 1189–1196.
26. Fett, T. and Munz, D., Evaluation of R-curve effects in ceramics. *Journal of Materials Science*, 1993, **28**, 742–752.
27. Fett, T., Evaluation of the bridging relation from crack-opening-displacement measurements by use of the weight function. *J. Am. Ceram. Soc.*, 1995, **78**(4), 945–948.
28. Bueckner, H. F., A novel principle for the computation of stress intensity factors. *ZAMM*, 1970, **50**(9), 529–546.
29. Hoffman, M., Fiedler, B., Köpke, U., Prielipp, H., Claussen, N. and Rödel, J. Toughening mechanisms of metal fibre reinforced ceramics. In *Fracture Mechanics of Ceramics Karlsruhe 1995*, Vol. 11 ed. R.C. Bradt, D.P.H. Hasselman, D. Munz, M. Sakai and V. Y. Shevchenko. Plenum Press, New York, 1996, pp. 177–188.
30. ASTM E399: Standard test method for plane–strain fracture toughness of metallic materials. *Annual Book of ASTM Standards*, Vol. 03.01, American Society for Testing and Materials, West Conshohocken, PA 1997, pp408-438.
31. Meschke, F., Raddatz, O., Kolleck, A. and Schneider, G.A., R-Curve behavior and crack closure stresses in $BaTiO_3$ and (Mg,Y)-PSZ ceramics. *J. Am. Ceram. Soc.*, 2000, **83**(2), 353–361.
32. Rice, J. R., Some remarks on elastic crack-tip stress fields. *Int. J. Solids Structures*, 1972, **8**, 751–758.

33. Tada, H., Paris, P. C. and Irwin, G. R., *The stress analysis of cracks handbook*. Del Research Corporation, Hellertown, 1973.
34. Fett, T. and Munz, D., *Stress Intensity Factors and Weight Functions*. Computational Mechanics Publications,, Ashurst, Southampton, 1997.
35. Knehans, R. and Steinbrech, R., Memory effect of crack resistance during slow crack growth in notched Al_2O_3 bend specimens. *Journal of Materials Science Letters*, 1982, **1**, 327–329.
36. Swanson, P. L., Fairbanks, C. J., Lawn, B. R., Mai, Y.-W. and Hockey, B. J., Crack–Interface grain bridging as a fracture resistance mechanism in ceramics: I, Experimental study on alumina. *J. Am. Ceram. Soc*., 1987, **70**(4), 279–289.
37. Hillig, B., Raddatz, O., Schneider, G.A. and Claussen, N. Analysis and model of the crack bridging mechanisms in a ductile fiber reinforced ceramic matrix composite. In preparation.
38. Hoffman, M., Skirl, S., Pompe, W. and Rödel, J., Thermal residual strains and stresses in Al_2O_3/Al composites with interpenetrating networks. *Acta Mater*, 1999, **47**(2), 565–577.
39. Marshall, D. B. and Evans, A. G., The Influence of residual stress on the toughness of reinforced brittle materials. *Materials Forum*, 1988, **11**, 304–312.
40. Knechtel, M. Präparation und Charakterisierung metallverstärkter Keramiken mit interpenetrierenden Netzwerken. Dissertation, Technische Universität Hamburg-Harburg, Hamburg, 1996.
41. Skirl, S. Mechanische Eigenschaften und Thermisches Verhalten von Al_2O_3/Al und Al_2O_3/Ni_3Al Verbundwerkstoffen mit Durchdringungsgefüge. Dissertation TU Darmstadt. In *Fortschritt-Berichte VDI* Reihe 5, Nr. 536, VDI-Verlag, Düsseldorf, 1998.
42. Fett, T. and Munz, D., Influence of initial crack size, specimen size and loading type on R-curves caused by bridging stresses. *Int. Journal of Fracture*, 1991, **49**, R21–R30.
43. Fett, T. and Munz, D., Influence of crack-surface interactions on stress intensity factor in ceramics. *J. Mat. Sci. Lett*., 1990, **9**, 1403–1406.
44. Cox, B. N. and Lo, C. S., Load ratio, notch, and scale effects for bridged cracks in fibrous composites. *Acta Metall. Mater*, 1992, **40**, 69–80.
45. Carpinteri, A., Cusp catastrophe interpretation of fracture instability. *J. Mech. Phys. Solids*, 1989, **37**(5), 567–582.
46. Biolzi, L., Cangiano, S., Tognon, G. and Carpinteri, C., Snap-back softening instability in high-strength concrete beams. *Materials and Structures*, 1989, **22**, 429–436.
47. Carpinteri, A. and Massabo, R., *Int. J. Solids and Structures*, 1997, **34**, 2321–2338.
48. Erdogan, F. and Joseph, P. F., Toughening of ceramics through crack bridging by ductile particles. *J. Am. Ceram. Soc*., 1989, **72**(2), 262–270.
49. Cox, B. N., Extrinsic factors in the mechanics of bridged cracks. *Acta Metall. Mater*, 1991, **39**(6), 1189–1201.
50. Cox, B. N. and Marshall, D. B., Stable and unstable solutions for bridged cracks in various specimens. *Acta Metall. Mater*., 1991, **39**(4), 579–589.
51. Cox, B. N. and Marshall, D. B., Overview No 111: concepts for bridged cracks in fracture and fatigue. *Acta Metall. Mater*., 1994, **42**(2), 341–363.